A Regional Seismic Array of Three-Component Stations in Central Saudi Arabia

Abdullah Al-Amri,[1] David Harris,[2,3] Mohammed Fnais,[1] Arthur Rodgers,[3] and Moustafa Hemaida[4]

INTRODUCTION

Seismic arrays are used to enhance signals and suppress noise as well as to estimate the slowness and azimuth of signals. Seismic monitoring traditionally has relied upon seismic arrays to reduce detection (magnitude) thresholds by increasing signal-to-noise ratios (SNR) and to contribute to event formation by improving phase identification and association. A seismic array differs from a local network of seismic stations mainly by the techniques used for data analysis. In principle, a network of seismic stations can be used as an array, and data from an array can be analyzed the same as from a network. However, most array processing techniques require high signal coherency across the array, and this puts important constraints on the array geometry, spatial extent, and data quality. Furthermore, proper analysis of array data is dependent on a stable, highly precise relative timing of all array elements. This is required because the measurement of (usually very small) time differences in the arrival of seismic signals between the different sensors plays an important role in all array processing techniques.

The Department of Geology of King Saud University (KSU) has established a small-aperture (~3.5 km) three-component seismic array in central Saudi Arabia at a hard rock site on the Arabian shield (Figure 1A). The facility consists of well-constructed vaults in hard rock outcrops in a region that has very low background noise. The deployed equipment consists of a broadband three-component sensor (STS-2) at the center element and eight short-period three-component sensors at the outlying elements (Figure 1B). The objectives of this deployment are to provide data for research into three-component seismic array processing and structural studies and are not related to any real-time monitoring efforts (*e.g.*, the International Monitoring System). Specifically, the array project is intended to improve constraints on the structure and physical state of the lithosphere beneath the Arabian shield and the Red Sea, to provide information concerning the tectonic evolution of the Arabian plate, to enhance existing models of the crust, and to provide additional constraints on seismicity in the region, especially at lower magnitudes, which we expect to lead to more complete and accurate earthquake catalogs. We anticipate improving velocity models of the crust, which we intend to use in investigations of attenuation, ultimately contributing to assessments of seismic hazard in the region. Better models of upper mantle structure may provide insights into the depth of the source of volcanism (the Harrats, Figure 1A) in the region and uplift of the Arabian shield.

Since this is the first array in the region designed for coherent regional signal processing and because so few seismic stations in the Middle East provide openly available broadband data, this array will provide unique and valuable data. This paper describes some preliminary analyses of the array data. We measured coherence of (regional and teleseismic) signals and noise as a function of inter-sensor separation and frequency. We also made slowness and azimuth measurements of regional and teleseismic phases and compared these to predictions from radial earth models to characterize path-specific propagation. We characterized background noise at the sites. Because few fully three-component arrays exist, we anticipate that data from the KSU array will contribute to the general understanding of processing strategies that combine beamforming with polarization analysis. We will also be interested to investigate the seasonal and diurnal noise spectral levels and frequency-dependent spatial structure (coherence and azimuthal dependence).

GEOLOGIC AND SEISMOTECTONIC SETTING

The accretionary evolution of the Arabian plate is thought to have originated and been formed by amalgamation of five Precambrian terranes. These are the Asir, Hijaz, and Midyan terranes from the western part of the Arabian shield, and the Afif terrane and the Amar arc of the Ar Rayn microplate from the eastern side of the shield. The western fusion is along the Bir Umq and Yanbu sutures (Looseveld *et al.* 1996). The eastern accretion may have started by about 680–640 million years ago (Ma) when the Afif terrane collided with the western shield along the Nabitah suture. At about 670 Ma, a subduction complex formed west of Amar arc. Along this subduction zone, the Afif terrane and Ar Rayn microplate collided around

---

1. Department of Geology, King Saud University, Riyadh, Saudi Arabia
2. Deschutes Signal Processing LLC, Maupin, Oregon, U.S.A.
3. Atmospheric, Earth and Energy Division, Lawrence Livermore National Laboratory, Livermore, California, U.S.A.
4. Research Institute of Petroleum and Gas, King Abdulaziz City for Science and Technology, Riyadh, Saudi Arabia
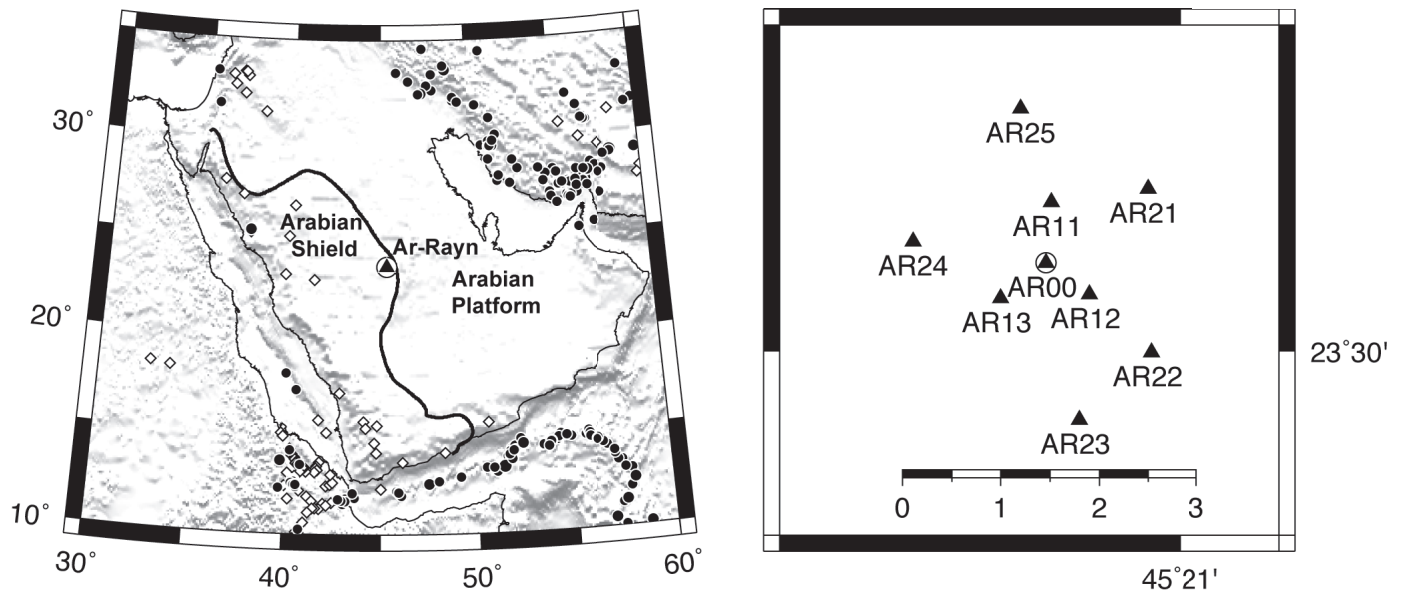
▲ **Figure 1.** (A) Location map of the Arabian plate showing major tectonic elements of the Arabian shield and platform (Al-Husseini 2000) and the position of the Ar Rayn seismic array (triangle). Earthquakes greater than magnitude 5 for the period 2000–2010 and volcanic centers are indicated by black circles and white diamonds, respectively. (B) The array geometry, which has a broadband sensor (STS-2) at its center (triangle with circle), surrounded by two rings of short-period sensors (triangles).

640–620 Ma. (Al-Husseini 2000). The north-trending Rayn anticlines and conjugate northwest and northeast fractures and faults may have formed at this time.

The Arabian shield is an ancient land mass with a trapezoidal shape and area of about 770,000 sq. km. Its slightly arched surface is a peneplain sloping very gently toward the north, northeast, and east. The framework of the shield is composed of Precambrian rocks and metamorphosed sedimentary rocks intruded by granites. The fold-fault pattern of the shield, together with some stratigraphic relationships, suggests that the shield has undergone two orogenic cycles. To the first order, the Arabian shield is composed of two layers, each about 20 km thick, with average velocities of about 6.3 km/s and 7 km/s respectively (Mooney *et al.* 1985). The crust thins rapidly to less than 20 km total thickness at the western shield margin, beyond which the sediments of the Red Sea shelf and coastal plain are underlain by oceanic crust.

The platform consists of the Paleozoic and Mesozoic sedimentary rocks that unconformably overlie the shield and dip very gently and uniformly to the east-northeast toward the Arabian Gulf (Powers *et al.* 1966). The accumulated sediments in the Arabian platform represent the southeastern part of the vast Middle East basin that extends eastward into Iran, westward into the eastern Mediterranean, and northward into Jordan, Iraq, and Syria.

The Arabian shield isolated the Arabian platform from the north African Tethys Sea and played an active paleogeographic role through gentle subsidence of its northern and eastern sectors during the Phanerozoic, allowing almost 5,000 m of continental and marine sediments to be deposited over the platform. This accumulation of sediments represents several cycles from

the Cambrian onward, and now forms a homocline dipping very gently away from the Arabian shield.

Several structural provinces can be identified within the Arabian platform: (1) an interior homocline in the form of a belt, about 400 km wide, in which the sedimentary rocks dip very gently away from the shield outcrops; (2) an interior platform, up to 400 km wide, within which the sedimentary rocks continue to dip regionally away from the shield at low angles; and (3) intra-shelf depressions, found mainly around the interior homocline and interior platform.

The Saudi Arabian Broadband Deployment (Vernon and Berger 1997; Al-Amri *et al.* 1999) provided the first broadband recordings for the Arabian shield and platform. This deployment consisted of nine broadband, three-component seismic stations along a transect similar to a seismic refraction study (Mooney *et al.* 1985; Gettings *et al.* 1986; Badri 1991). Data from this deployment resulted in several reports of crustal and upper mantle structure (Sandvol *et al.* 1998; Mellors and Vernon 1999; Rodgers *et al.* 1999; Benoit *et al.* 2003; Mokhtar *et al.* 1997). The crustal model of the western Arabian platform shows a slightly higher *P* velocity for the upper crust in the Arabian shield than in the platform. Also the crust of the platform appears to be 3–5 km thicker than in the shield. The Moho discontinuity beneath the western Arabian platform occurs at a depth of 40–45 km, and the velocity of the upper mantle is about 8.2 km/sec (Al-Amri 1998, 1999; Rodgers *et al.* 1999; Tkalčić 2006).

Generally, the crustal thickness in the Arabian shield varies from about 15 km in the Red Sea to 20 km along the Red Sea coast to about 35–40 km in the central Arabian shield (Sandvol *et al.* 1998; Al-Damegh *et al.* 2005; Tkalčić 2006). Large-scale

▲ **Figure 2.** Station sites were chosen for Precambrian bedrock contact. Site preparation included excavation to undisturbed bedrock with heavy equipment.

seismic tomography (*e.g.*, Debayle *et al.* 2001) suggests that a low-velocity anomaly in the upper mantle extends laterally beneath the Arabian shield from the Red Sea in the west to the shield-platform boundary in the east. Additionally, Debayle *et al.* (2001) observed a narrow region of low velocity beneath the Red Sea and the western edge of the Arabian shield, extending to 650 km depth. Recent tomographic imaging by Park *et al.* (2007) using Saudi Arabian National Digital Seismic Network data found low velocities extending to 400 km in the upper mantle beneath the southern Red Sea and Arabian shield but more normal velocities beneath the northern Red Sea, suggesting different geodynamic connections between rifting of the Red Sea and mantle upwelling in the southern and northern Red Sea.

High-frequency regional *S*-wave phases are quite different for paths sampling the Arabian shield than those sampling the Arabian platform (Mellors and Vernon 1999; Al-Damegh *et al.* 2004; Pasyanos *et al.* 2009). In particular the mantle *Sn* phase is nearly absent for paths crossing parts of the Arabian shield, while the crustal *Lg* phase has abnormally large amplitude. This may result from an elastic propagation effect or extremely high mantle attenuation and low crustal attenuation occurring simultaneously, or a combination of both. High-frequency *Lg* does not propagate as efficiently across the Arabian platform compared to the shield, but *Sn* does propagate efficiently. This observation suggests that crustal attenuation is low in the higher velocity crust of the Arabian shield or that sedimentary structure in the Arabian platform attenuates and disrupts the crustal waveguide for *Lg*. These observations imply that high-frequency ground motions will propagate with lower attenuation in the Arabian shield than in the Arabian platform.

INSTALLATION AND PRELIMINARY NOISE RESULTS

Great care was taken to site the stations of the Ar Rayn array on Precambrian outcrops. Figure 2 shows a representative station site (AR25). Note that the station is sited adjacent to an outcrop where it was possible to excavate a vault into contact with undisturbed Precambrian bedrock. The inside dimensions of the vault are 1.6 m square and 2 m deep (Figure 3). At the bottom a 1.4 m × 1.4 m concrete pier, 2 m deep, was poured directly on bedrock. This dimension affords a 10-cm separation between the pier and the walls of the vault for noise isolation. The walls themselves are composed of two shells: a concrete block wall on the outside, with foam filling the voids of the blocks for thermal isolation; and a 20-cm inside wall poured of solid concrete. Neither of the walls contains any steel reinforcement to prevent possible noise contributed to the motion of the mass. The top of the vault is covered by a double door with 10 cm of foam for thermal isolation. The walls and top of the vaults are flush with the ground surface to minimize wind noise. The 80-watt solar panel is mounted close to the ground surface, also to minimize wind noise that would be transmitted into the vault if a mast mounting had been used.
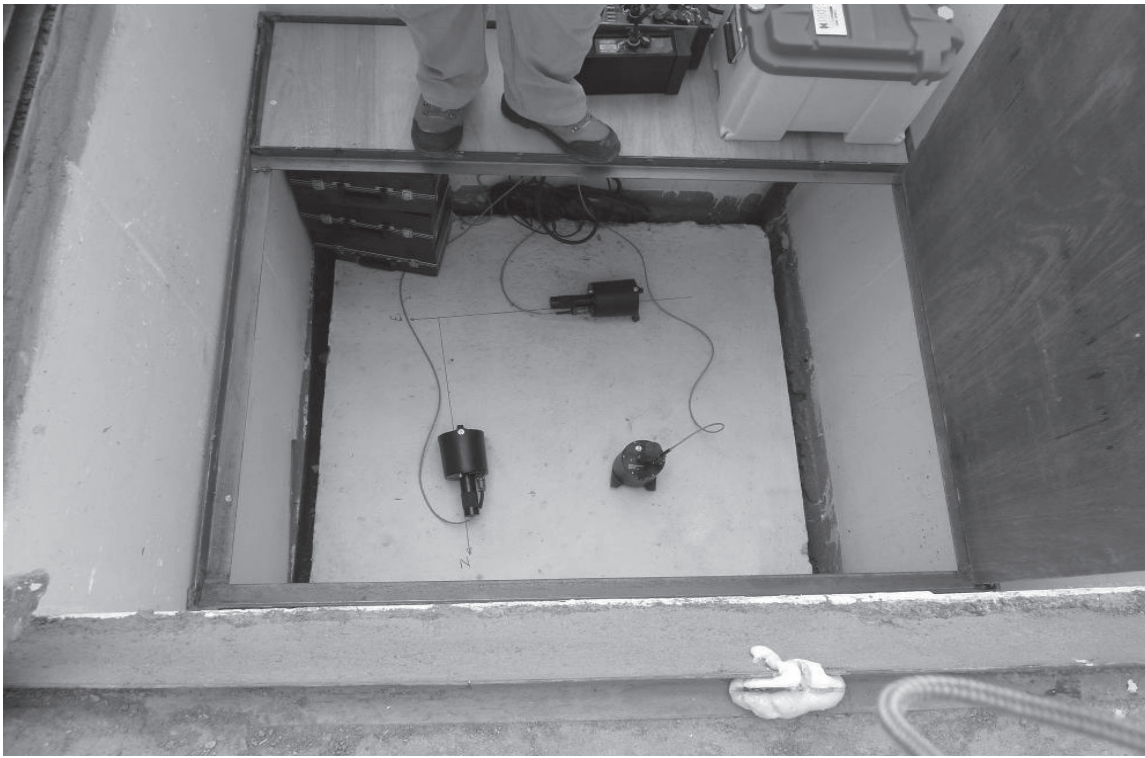
▲ **Figure 3.** Typical vault installation of a short-period three-component instrument. The concrete pier was poured directly on bedrock.

The short-period instruments are Kinemetrics SS-1 Ranger seismometers (1-Hz free period). Three are arranged in a three-component configuration as shown in Figure 3. The data are acquired by Quanterra Q330 data loggers and stored on Bailer 44 data storage devices with 32 gigabytes of flash memory. The sampling rate is 100 samples per second for each channel. The single broadband sensor at the center of the array (AR00) is a Streckeisen STS-2. Otherwise the configuration of this installation is the same as the short-period stations.

Figure 4 shows the noise level as a function of frequency for the three components of the broadband center element of the array, following the format of Astiz (1997). The vertical axis is acceleration power expressed in decibels with respect to 1 m^2/s^4/Hz. The gray lines denote the U.S. Geological Survey low and high noise models of Peterson (1993). Low-frequency noise levels are close to the low noise model at 0.1 Hz and noise increases as frequency decreases. This may be corrected by improving the vault construction (*e.g.*, deeper emplacement, thermal isolation). At mid-level and higher frequencies (0.1–10 Hz), the three noise spectra lie near the USGS low noise model. The high frequency noise, especially the distinct spectral lines, could be instrument noise or cultural noise from the nearby town of Ar Rayn, which is 15 km from the array.

In general, noise levels are similar for all channels for frequencies greater than 1 Hz. Between 1 Hz and roughly 0.1 Hz, the vertical is slightly noisier than the horizontals. At frequencies less than 0.1 Hz, the horizontal components are much noisier, creating an obvious discrepancy with the low-noise model. The long-period noise levels on the horizontal channels may present a problem for surface wave studies

and regional moment tensor inversions, which are forced to depend solely on vertical data for moderate-sized events. The source of the noise is not clear. One possibility is that the long-period noise may be due to small tilts that affect the horizontal more than the verticals because horizontal tilts greatly increase the effect of the local gravity vector. Tilt effects can be quite large compared to the signals normally recorded, and may be due to prevailing winds and/or transient thermal effects caused by large diurnal temperature variations in the desert.

The body-wave magnitude (*mb*) detection threshold for the distance range of 10–100 degrees is about $m_b > 3.5$ (Vernon and Berger 1997). Minimum detectable magnitudes are estimated for RAYN station using the observed noise levels over 1 Hz. The m_b detection threshold for the distance range of 5–10 degrees is about 2.7–3.0, assuming the signal-to-noise ratio of 3 dB or better (Al-Amri *et al.* 1999). Al-Amri and Al-Amri (1999) indicated that seasonal noise levels varied at RAYN, with April to June the quietest, and October to December the noisiest, months. Slight changes in peak microseism frequency also occurred seasonally. Absolute noise levels near the microseism frequency (0.1 to 0.2 Hz) were about equal for all seasons at -140 dB. Above 1Hz, RAYN station shows an increase in seasonal variations from -140 dB in the summer to -160 dB in the winter. Mellors (1998) showed that noise levels at nine broadband stations (STS-2) across the Arabian shield are similar for all channels for a given station for frequencies greater than 0.9 Hz. Between 0.9 Hz and roughly 0.1 Hz, the vertical is slightly noisier than the horizontals, and at frequencies less than 0.1 Hz, the horizontals are much noisier.
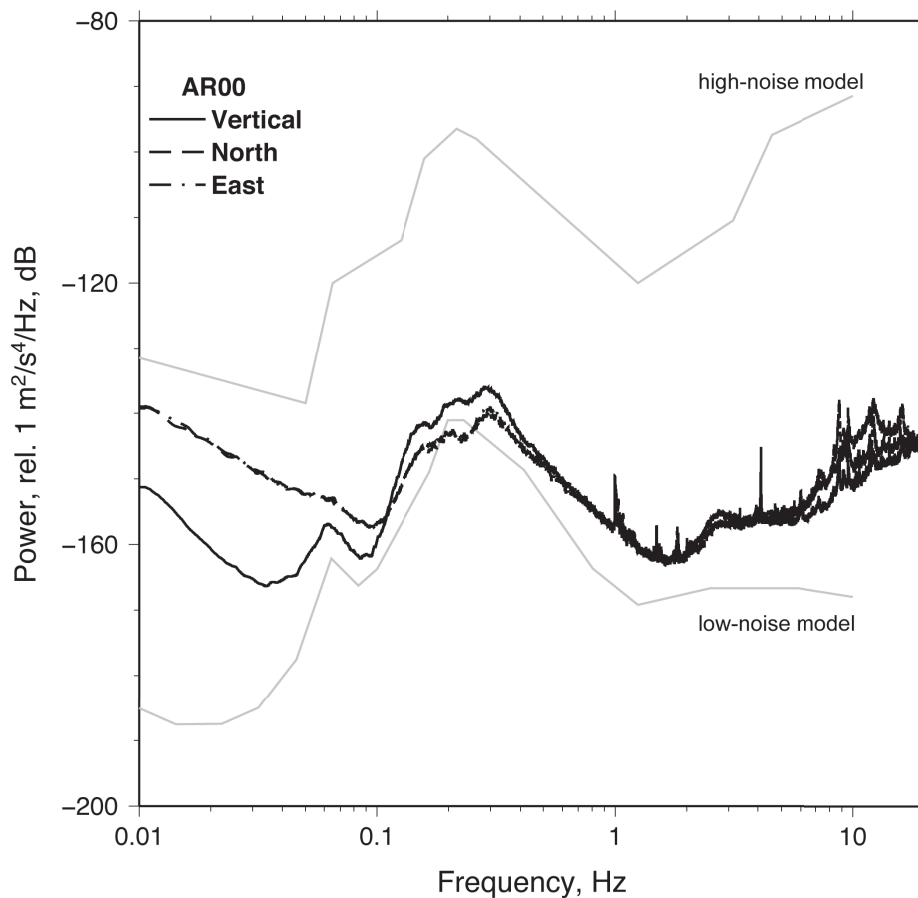
▲ **Figure 4.** Average ambient noise levels for the three components of the central broadband element AR00 (vertical, north, and east as solid, dashed, dashed-dotted lines, respectively). The noise power spectral densities are expressed in acceleration power relative to 1 m²/s⁴/Hz in decibels (dB). Reported low and high noise models from Peterson (1993) are shown as gray lines.

PRELIMINARY DATA PROCESSING

We show three signal processing examples using Ar Rayn array data. The first is a check of coherence using a teleseismic observation of an m_b 5.3 earthquake in the vicinity of Greece (USGS preliminary hypocenter 38.425 N and 44.022 E, depth 10 km) that occurred on 22 January 2010 at 00:46:57.5 GMT. Figure 5 (left) displays the vertical waveforms of seven of the array short-period elements in a 30-second window about the initial P phase filtered 1–3 Hz. Figure 5 (right) shows a frequency-wavenumber (FK) spectrum computed from that P phase. The backazimuth (-63.4 degrees) and phase velocity (10.2) values estimated from the spectral peak were used to align the signals for a coherence analysis. That analysis is shown in Figure 6, with the aligned P waveforms on the top and, on the bottom, the correlation values of all 21 distinct pairs of signals plotted as a function of sensor separation. The correlation values are quite high, as is expected for a low-frequency (~Hz) teleseismic P phase observed across a 3-km aperture. Nonetheless, the high correlation values indicate desirable uniformity of vault installation, coupling to bedrock, site response, and instrumentation.

An interesting observation of a local event is shown in Figures 7 through 9. This is a local magnitude 2.3 (King Abdulaziz City for Science and Technology [KACST] cata-log) event that occurred approximately 260 km NNE of the array. Only the Lg phase is clear in the data (Figure 7) filtered into the 0.8 to 3 Hz band. There is a hint of a P phase approximately 30 seconds before the Lg signal, but no distinct arrival can be reliably picked. Higher frequency filter bands do not improve the signal-to-noise ratio in this case. A wideband (1–3 Hz) FK spectrum of the Lg arrival (Figure 8) provides a usable backazimuth and a phase velocity (3.79 km/s) confirming the identity of the Lg phase. The measured Lg backazimuth and an assumed phase velocity of 8 km/s can be used to search for the P-phase arrival. Figure 9 shows an individual vertical waveform (top trace) and the P beam (middle trace). The (probable) Pn phase now is clearly visible. Still greater processing gain can be obtained for the P phase by combining beamforming and polarization filtering. The third trace in the figure shows a polarized beam obtained by forming separate beams on the vertical, north, and east components of the array, then rotating the resulting three-component beam set onto the polarization vector of Pn for this event (backazimuth 29.5 degrees, angle of incidence 39 degrees). The angle of incidence used assumes a near-surface medium P-wave velocity of 5 km/s. This processing approach roughly doubles the signal-to-noise ratio of the incident P wave relative to the vertical beam, enhancing our ability to pick and identify this phase.
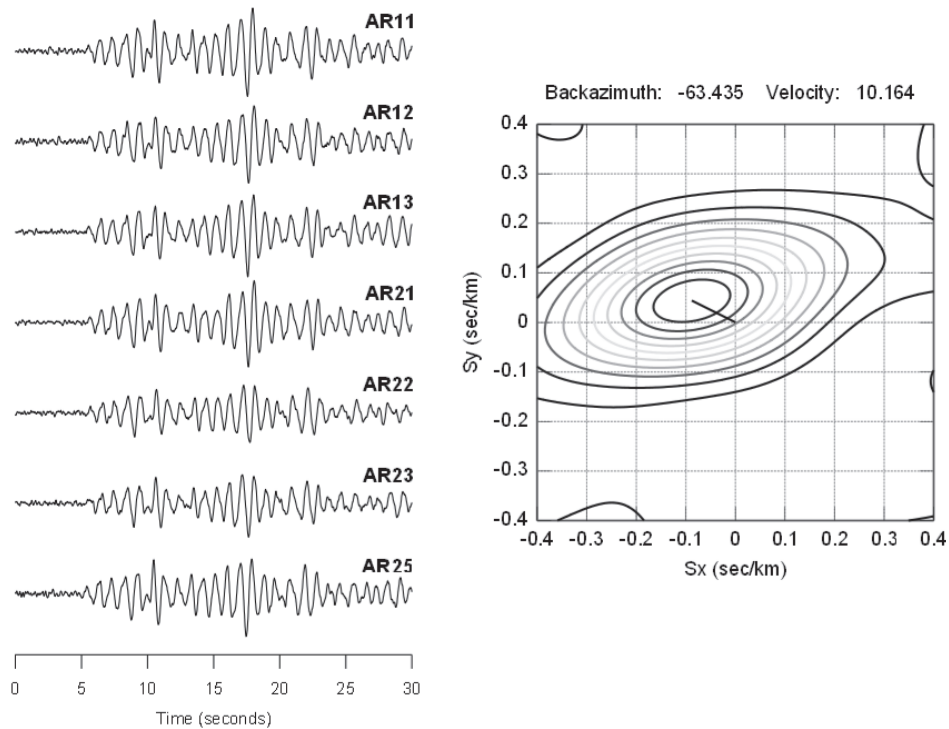
▲ **Figure 5.** FK spectrum, computed between 1 and 3 Hz, of the initial *P* phase for an earthquake in the vicinity of Greece that occurred on 22 January 2010. The cut *P*-phase waveforms are shown at left and the FK spectrum to the right. Coherence of this phase is high, as is expected of a teleseismic observation; the measured backazimuth and phase velocity are used to align the waveforms for a coherence measurement.
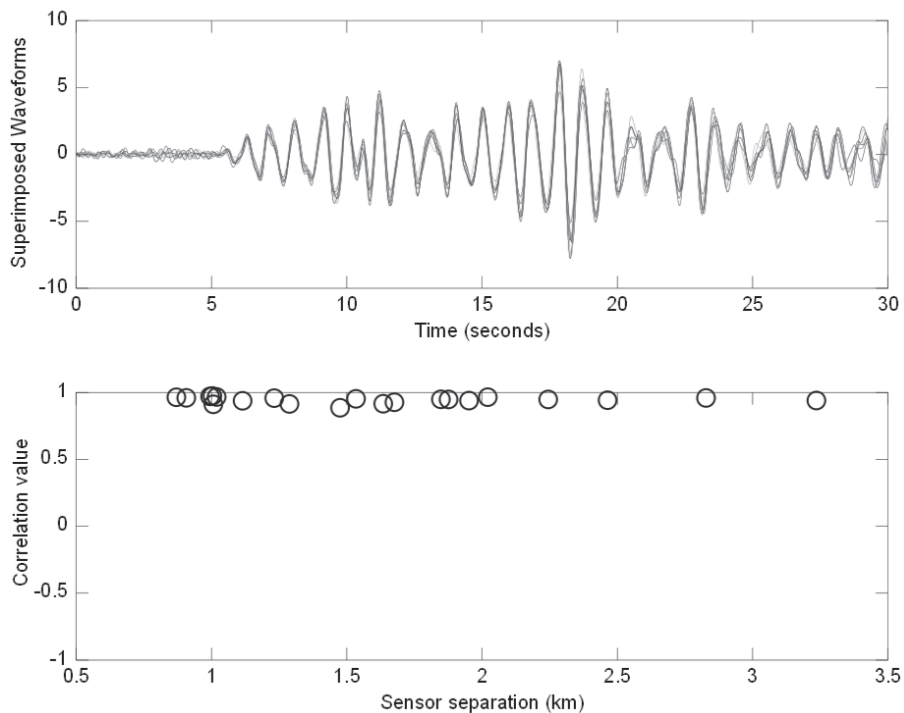

▲ **Figure 6.** Coherence of the teleseismic *P* phase at the array is high, demonstrating uniformity of installation and instrumentation. At top, the *P* waves of the teleseism from Greece are superimposed to show the domain of calculation of signal correlation. At the bottom, the 21 correlation coefficients between unique pairs of sensors are shown plotted as a function of sensor separation. The *P* phase is relatively narrowband, with most of its energy just above 1 Hz. Therefore coherence is expected to be high, but nonetheless indicates proper installation of the instrumentation.
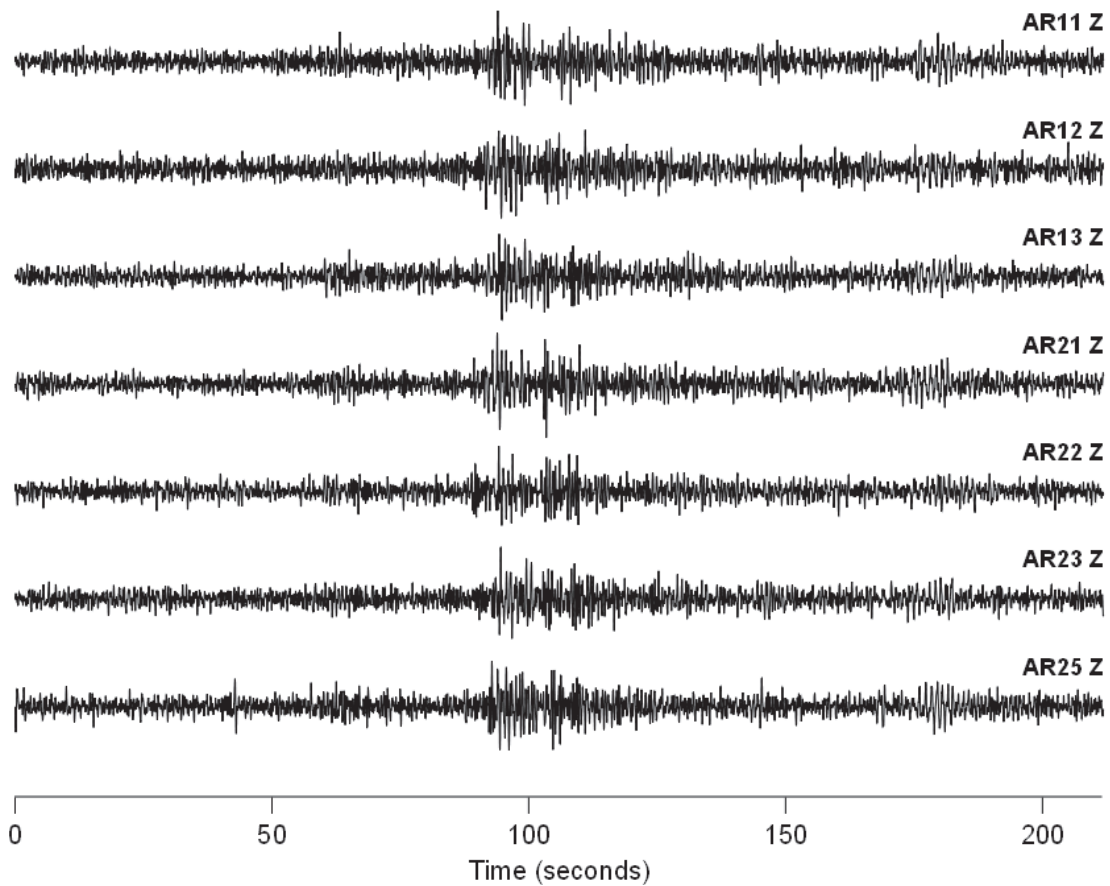
▲ **Figure 7.** This small central Arabian event about 260 km from the array has a low SNR that makes observation of the *P* phases difficult. A window around the *Lg* phase from 90 to 100 s allows backazimuth estimation with an FK spectrum.
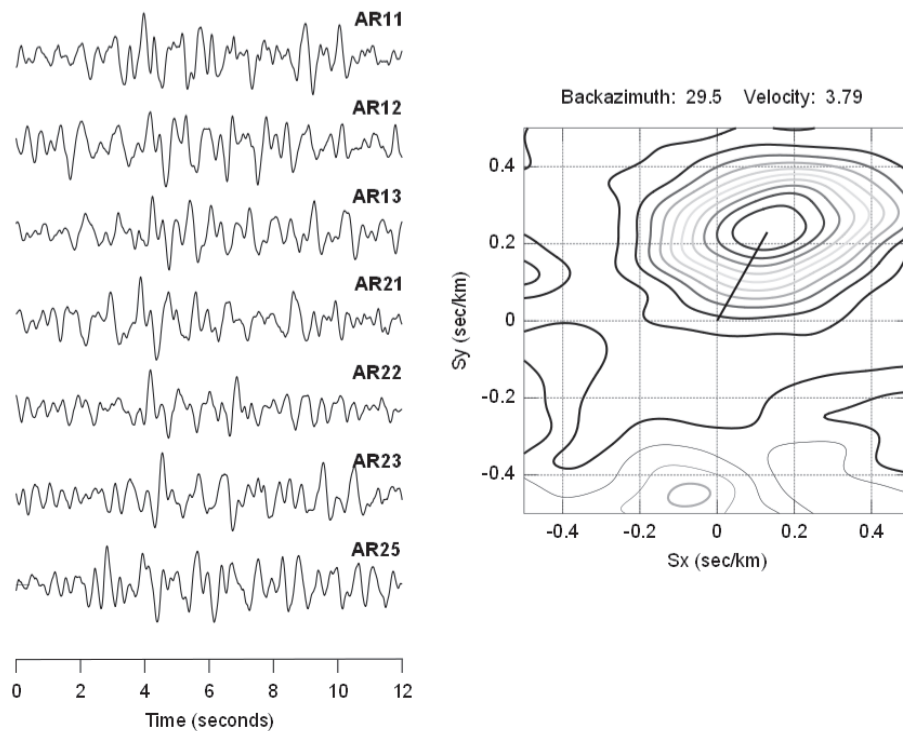
▲ **Figure 8.** An FK spectrum of the *Lg* phase of the small central Arabian event provides a usable backazimuth. The measured phase velocity is consistent with *Lg* propagation.
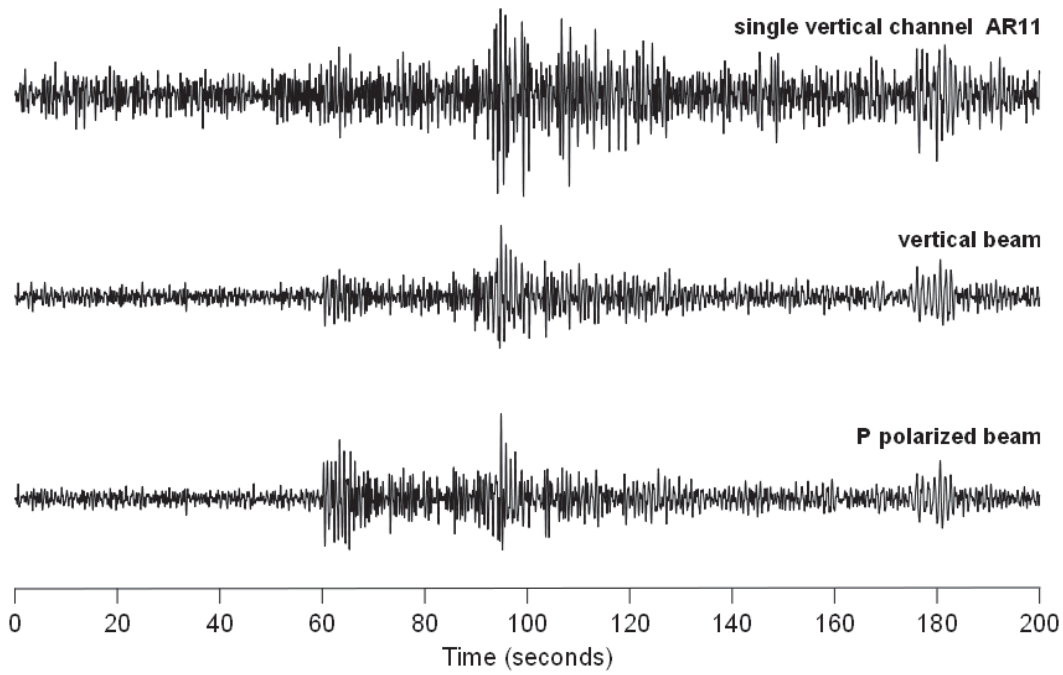
▲ **Figure 9.** Beamforming greatly enhances our ability to interpret the *P* phase of this small central Arabian event. The top trace is the waveform from a single vertical sensor of the array filtered into the 0.8 to 3 Hz band. The second trace is the conventional beam made with the vertical elements of the array, using the *Lg* backazimuth (29.5 degrees) and an assumed *Pn* phase velocity of 8 km/s. The third trace is the beam formed from all seven three-component traces, assuming polarization consistent with *Pn* (*P* medium velocity of 5 km/s; incidence angle of 39 degrees).

The three-component beam may be summarized mathematically by:

$$b(t) = \frac{1}{N} \mathbf{c} \sum_{i=1}^{N} \mathbf{r}_i(t - \Delta_i) ,\qquad(1)$$

where bold quantities are vectors. The vector of three-component signals recorded at station i is denoted by:

$$\mathbf{r}_i(t) = \begin{bmatrix} \mathbf{z}_i(t) \\ \mathbf{n}_i(t) \\ \mathbf{e}_i(t) \end{bmatrix},\qquad(2)$$

where the triple $\{\mathbf{z}_i(t), \mathbf{n}_i(t), \mathbf{e}_i(t)\}$ represents the vertical, north, and east components of the station. N is the number of stations in the array, and the propagation delays $\{\Delta_i\}$ are described by a plane wave model:

$$\Delta_i = \mathbf{s} \cdot \mathbf{x}_i .\qquad(3)$$

The vector $\mathbf{s}$ is the horizontal slowness vector, s is scalar horizontal slowness (ray parameter), and $\mathbf{c}$ is the polarization vector for P waves:

$$\mathbf{s} = s \begin{bmatrix} \cos\theta \\ \sin\theta \end{bmatrix} \qquad \mathbf{c} = \begin{bmatrix} \cos\varphi \\ \sin\varphi \, \cos\theta \\ \sin\varphi \, \sin\theta \end{bmatrix}\qquad(4)$$

where θ is the azimuth of propagation of north through east and φ is the angle of incidence with the vertical axis. Finally, the vector $\mathbf{x}_i$ represents the horizontal offset of station i from a common reference point.

Our final example of beamforming is an extraction of crustal and upper mantle P phases for an event in the Harrat Lunayyir volcanic center (25.215N 37.796E), approximately 790 km from the array. The event occurred on 15 April 2010 (04:10:04.25 GMT) and was estimated to be a magnitude 3.7 event by the Saudi Geological Survey. Figure 10 shows single channel recordings and beams for this event. The top trace is a vertical channel (station AR11) filtered into the 1–4 Hz band. A pronounced Lg phase is apparent, preceded by approximately 110 seconds by a very weak P phase. The three bottom traces in the figure are detailed views around the P phases, with the first of the three being again the filtered single vertical trace. The second trace is the beam formed from the vertical components only, and the third trace is the three-component beam (Equation 1). Note that, as with the smaller near-regional event, the three-component beam roughly doubles the power *SNR* for the *Pn* phase. *Pg* also is more clearly visible on this beam, arriving about 14 s after *Pn*.

SUMMARY

Based on the background noise level observed at the center element of the Ar Rayn seismic array, coherence analysis, and beam-forming results for representative events in the region, this array of data should prove very valuable for examining
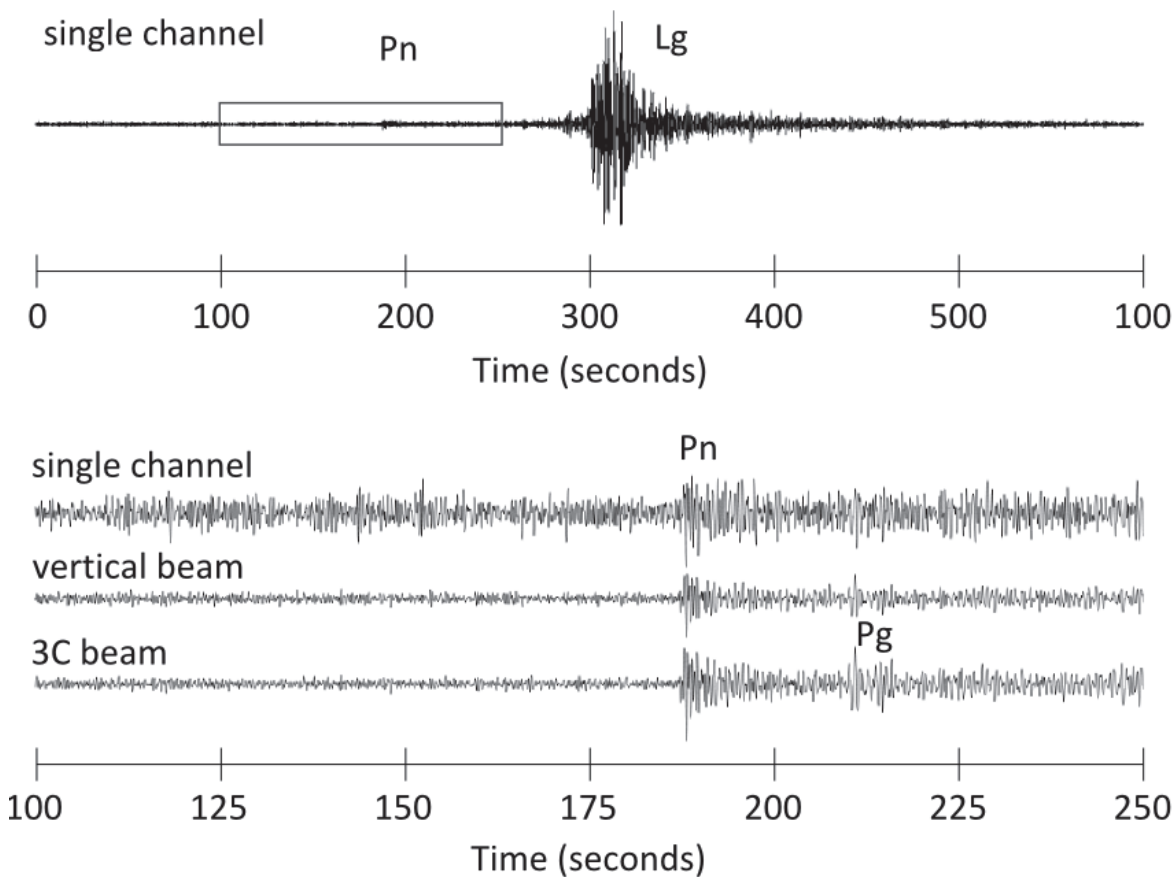
▲ **Figure 10.** Result of beamforming for the initial *P* phases of a magnitude 3.9 event at the Harrat Lunayyir volcanic field approximately 790 km from the array. The top trace is a single short-period vertical channel filtered into the 1–4 Hz band. The signal is dominated by *Lg*, but a small *Pn* arrival is visible around 190 s. Below are detailed traces referenced to the boxed interval of the top trace. These traces display again the filtered single trace, a vertical beam on the *Pn* velocity and backazimuth, and a three-component beam. The beams show the *Pn* arrival more clearly, and the three-component beam also provides a clearer view of the *Pg* arrival.

seismicity and structure in the Arabian peninsula. Noise levels approach the Peterson low noise model (1993) between 0.05 Hz and 2 Hz and are low in the 2–10 Hz band. Noise levels are elevated on the horizontal elements below 0.05 Hz, which may limit measurements of surface wave dispersion and moment tensor inversions but should not affect high-frequency beamforming capabilities.

Initial beamforming results demonstrate that the array will improve estimates of *P* arrival times and waveforms for small events in the region. Since the array is one of only a few with three-component stations deployed at all elements, it should provide opportunities to examine more sophisticated combinations of beamforming and polarization filtering and phase identification and association through three-component FK analysis. Initial results for two events, one at local distance and a second at regional distance, confirm this expectation. ◪

ACKNOWLEDGMENTS

REFERENCES

Al-Amri, A. M. (1998). The crustal structure of the western Arabian platform from the spectral analysis of long-period *P*-wave amplitude ratios. *Tectonophysics* **290**, 271–283.

Al-Amri, A. M. (1999). The crustal and upper-mantle structure of the interior Arabian platform. *Geophysical Journal International* **136**, 421–430.

Al-Amri, A. M., P. Davis, M. Al-Amri, A. Gharib, and J. Berger (1999). Seismic characteristics of RAYN/ GSN station, Saudi Arabia. *Journal of King Saud University: Science* **2**, 81–92.

Al-Amri, A. M., R. Mellors, and F. Vernon (1999). Broadband seismic noise characteristics of the Arabian shield. *The Arabian Journal for Science and Engineering* **24** (2A), 99–113.

Al-Damegh, K., E. Sandvol, and M. Barazangi (2005). Crustal structure of the Arabian plate: New constraints from the analysis of teleseis-

mic receiver functions. *Earth and Planetary Science Letters* **231**, 177–196.

Al-Dameigh, K., E. Sandvol, A. Al-Lazki, and M. Barazangi (2004). Regional wave propagation (*Sn* and *Lg*) and *Pn* attenuation in the Arabian plate and surrounding regions. *Geophysical Journal International* **157**, 775–795.

Al-Husseini, M. I. (2000) Origin of the Arabian plate structures: Amar collision and Najd rift. *GeoArabia* **5**, 527–542.

Astiz, L. (1997). *How to Estimate Power Spectral Density of Seismic Noise for FDSN Broadband Digital Stations.* USGS Open-File Report 93-322, 95 pp.

Badri, M. (1991). Crustal structure of central Saudi Arabia determined from seismic refraction profiling. *Tectonophysics* **185**, 357–374.

Benoit, M., A. Nyblade, J. VanDecar, and H. Gurrola (2003). Upper mantle *P*-wave velocity structure and transition zone thickness beneath the Arabian shield. *Geophysical Research Letters* **80**; doi:10.1029/2002GL016436.

Debayle, E., J. Leveque, and M. Cara (2001). Seismic evidence for a deeply rooted low-velocity anomaly in the upper mantle beneath the northeastern Afro/Arabian continent. *Earth and Planetary Science Letters* **193**, 423–436.

Gettings, M., H. Blank, W. Mooney, and J. Healey (1986). Crustal structure of southwestern Saudi Arabia. *Journal of Geophysical Research* **91**, 6,491–6,512.

Looseveld, R. J. H., A. Bell, and J. J. M. Terken (1996). The tectonic evolution of interior Oman. *GeoArabia* **1**, 28–51.

Mellors, R. (1998). *Preliminary Noise Survey and Data Report of Saudi Arabian Data.* Lawrence Livermore National Laboratory, technical report, UCRL-ID-128949.

Mellors, R., and F. Vernon (1999). *Analysis of Data from the Broadband Saudi Arabian Deployment.* Final report to Lawrence Livermore National Laboratory, 29 pp.

Mokhtar, T., C. Ammon, H. Ghalib, and R. Herrmann (1997). Lithospheric structure beneath Arabia. *Eos, Transactions, American Geophysical Union* **78**, F499.

Mooney, W., M. Gettings, H. Blank, and J. Healy (1985). Saudi Arabian seismic refraction profile: A traveltime interpretation of crustal and upper mantle structure. *Tectonophysics* **111**, 173–246.

Park, Y., A. Nyblade, A. Rodgers, and A. M Al-Amri (2007). Upper mantle structure beneath the Arabian Peninsula from regional body-wave tomography: Implications for the origin of Cenozoic uplift and volcanism in the Arabian shield. *Geochemistry, Geophysics, Geosystems* **8**; doi:10.1029/2006GC001566.

Pasyanos, M. P., W. R. Walter, and E. M. Matzel (2009). A simultaneous multiphase approach to determine *P*-wave and *S*-wave attenuation of the crust and upper mantle. *Bulletin of the Seismological Society of America* **99**, 3,314–3,325.

Peterson, J. (1993). *Observations and Modeling of Seismic Background Noise.* USGS Open-File Report 93-322. Albuquerque, NM, 94 pp.

Powers, R. W., L. F. Ramirez, C. D. Redmond, and E. L. Elberg (1966). *Sedimentary Geology of Saudi Arabia,* in *Geology of the Arabian Peninsula.* USGS professional paper 560-D D1-D147. Washington, DC: U.S. Government Printing Office.

Rodgers, A., W. Walter, R. Mellors, A. M. S. Al-Amri, and Y. S. Zhang (1999). Lithospheric structure of the Arabian shield and platform from complete regional waveform modeling and surface wave group velocities. *Geophysical Journal International* **138**, 871–878.

Sandvol, E., D. Seber, M. Barazangi, F. Vernon, R. Mellors, and A. Al-Amri (1998). Lithospheric seismic velocity discontinuities beneath the Arabian shield. *Geophysical Research Letters* **25**, 2,873–2,876.

Tkalčić, H., M. Pasyanos, A. Rodgers, R. Gok, and A. Al-Amri (2006). A multi-step approach for joint modeling of surface wave dispersion and teleseismic receiver functions: Implications for lithospheric structure of the Arabian Peninsula. *Journal of Geophysical Research* **111**, B113111; doi:10.1029/2005JB004130.

Vernon, F., and J. Berger (1997). *Broadband Seismic Characterization of the Arabian Shield.* Final Scientific Technical Report, Department of Energy Contract No. F 19628-95-K-0015, 36 pp.

Atmospheric, Earth and Energy Department
Lawrence Livermore National Laboratory
7000 East Avenue
Livermore, California 94551 U.S.A.
rodgers7@llnl.gov
(A. R.)